Proceedings of ASME-IMECE'07
2007 ASME International Mechanical Engineering Congress and RD&D Expo
November 11-15, 2007, Seattle, Washington USA

IMECE2007-42559

HIGH SPEED ROTARY PULSE WIDTH MODULATED ON/OFF VALVE *

Haink C. Tu, Michael B. Rannow, James D. Van de Ven, Meng Wang, Perry Y. Li† and Thomas R. Chase
Center for Compact and Efficient Fluid Power
Department of Mechanical Engineering
University of Minnesota
111 Church St. SE
Minneapolis, MN 55455
Email: {tuxxx021,rann0018,vandeven,wang134,pli,trchase}@me.umn.edu

ABSTRACT

A key enabling technology to effective on/off valve based control of hydraulic systems is the high speed on/off valve. High speed valves improve system efficiency for a given PWM frequency, offer faster control bandwidth, and produce smaller output pressure ripples. Current valves rely on the linear translation of a spool or poppet to meter flow. The valve spool must reverse direction twice per PWM cycle. This constant acceleration and deceleration of the spool requires a power input proportional to the PWM frequency cubed. As a result, current linear valves are severely limited in their switching frequencies. In this paper, we present a novel fluid driven PWM on/off valve design that is based on a unidirectional rotary spool. The spool is rotated by capturing momentum from the fluid flow through the valve. The on/off functionality of our design is achieved via helical barriers that protrude from the surface of a cylindrical spool. As the spool rotates, the helical barriers selectively channel the flow to the application (on) or to tank (off). The duty ratio is controlled by altering the axial position of the spool. Since the spool no longer accelerates or decelerates during operation, the power input to drive the valve must only compensate for viscous friction, which is proportional to the PWM frequency squared. We predict that our current design, sized for a nominal flow rate of $40l/m$, can achieve a PWM frequency of $84Hz$. This paper presents our valve concept, design equations, and an analysis of predicted performance. A simulation of our design is also presented.

1 Introduction

On/off (or digital) valve based control of hydraulic systems is an energy efficient alternative to control via throttling valves. In either the on or the off state, energy loss is minimized since either the pressure drop across the valve is small or the flow through it is zero. When the on/off valve is pulse width modulated (PWM), the average pressure or flow can be controlled. Our previous papers [6] and [5] have proposed and modeled the use of a PWM on/off valve with a fixed displacement pump and an accumulator to achieve the functionality of a variable displacement pump. A critical requirement for practical on/off valve based control is the availability of high speed on/off valves. High speed valves improve system efficiency for a given PWM frequency, increase control bandwidth, and reduce output pressure ripple. Commercial on/off valves typically have transition times on the order of $20ms$ for flow rates of $5l/m$-$40l/m$. Digital valve control with current valves demonstrates a noticeable decrease in system efficiency when operating at PWM frequencies greater than $10Hz$ [5]. A limitation in conventional valve designs based on linear spool or poppet movement is that the spool/poppet must be started and stopped during each on/off cycle. The power required to actuate the valve is proportional to the $3rd$ power of the PWM frequency. In this paper, we present a novel fluid driven unidirectional rotary PWM on/off valve design. Our valve spool achieves rotary motion by capturing momentum from the fluid that it meters. Since the spool rotates at a near constant velocity, the power required to drive the valve only needs to overcome viscous friction, which is proportional to the frequency squared.

On/off valves have traditionally suffered from the trade off between switching speed and flow rate/pressure drop. Linear designs in particular are subject to this constraint due to the increased size and mass of the spool/poppet needed to handle larger flow rates. Typical high speed linear valve designs utilize piezoelectric materials or high speed solenoids for spool/poppet actuation, with a second pressure actuated stage if higher flow rates are required. Yokota et al. [7] presented a design in 1991 that used two multilayered piezoelectric actuators in a push-pull type configuration to actuate a poppet, achieving switching times on the order of $.1ms$. While this switching time is impressive, the valve exhibited a pressure drop of $10 \times 10^6 Pa$ for a flow rate of $7.2l/m$. Yokota et al. also proposed the use of this piezoelectric valve as a pilot stage to a secondary spool valve, however no information was given to the performance of this design. In 1994, Kajima et al. presented a high speed solenoid valve design capable of a switching time of $1ms$ [8]. In 2002, Lu et al. [9] presented a single stage 3-way piezoelectric hydraulic poppet valve capable of flow rates of $8l/m$ with on/off times on the order of $1.5ms$, while in 2004, Shi et al. [10] achieved an on/off time on the order of $1.5ms$ for a flow rate of $1.24l/m$ using a rare-earth-alloy giant magnetostrictive actuator to drive a linear valve spool. This magnetostrictive valve was then coupled with a second stage ball valve to achieve a two stage design capable of $8-10ms$ on/off times for a flow rate of $120l/m$ [11]. On/off valves that feature a rotary spool typically improve upon this trade off. Since less energy is required to actuate a rotary design for high switching speeds, the valve spool can be made larger, thus enabling higher flow rates at lower pressure drops. Cui et al. [14], in 1991, introduced the concept of a coupled rotary two stage hydraulic valve. The first stage of the valve consisted of a bidirectional rotary spool which generated pressure forces to move the spool axially. The axial motion of the spool opened and closed a second stage poppet which was integrated onto the end of the spool. This design was capable of achieving on/off times of $2.5ms$ with a nominal flow rate of $18l/m$. In 1993, Royston et al. [13] proposed a rotary pneumatic PWM on/off valve. The design utilized a unidirectional inner shaft driven by a DC motor to generate the on/off pulses with a bidirectional outer rotor to actuate the duty ratio of the valve. This valve was capable of PWM frequencies around $80Hz$. In 1980, Cyphelly et al. [12] proposed an externally actuated unidirectional 2-way hydraulic rotary spool valve that featured a helical profile on the spool surface. Our design utilizes a similar geometry, however our spool incorporates a 3-way design with integrated turbines that capture momentum from the fluid flow to spin the valve spool. By harvesting momentum from the metered fluid to spin the spool, we can eliminate the complex coupling of a mechanically actuated design. Additionally, the trade off between switching speed and flow rate is greatly reduced: as the flow rate through the valve is increased, inherently more momentum is available to spin the spool, although the size of the spool must be increased, increasing viscous friction.

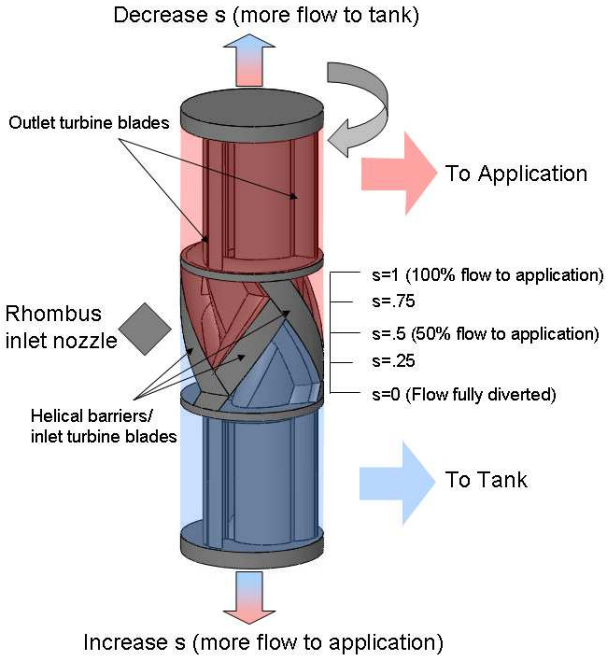

Figure 1. Diagram of 3-way rotary spool

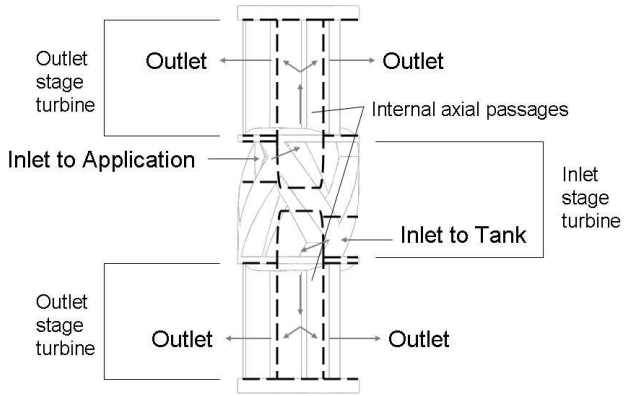

Figure 2. Diagram of internal geometry

This paper presents the concept and design of a unidirectional fluid driven rotary on/off valve. Section 2 introduces the functionality and design features of our concept. Section 3 provides an analysis of our design including calculations for performance and efficiency. A complete system simulation is presented in Section 4, and some concluding remarks are discussed in Section 5.

2 Self-spinning, 3-way Rotary on/off Valve Concept

Our self-spinning, 3-way rotary on/off valve concept is presented in Fig. 1. The valve spool consists of a central PWM section sandwiched by two outlet turbines. The central section

contains alternating helical barriers overlayed onto the spool surface. The helical barriers partition the spool into regions where flow is directed to the application (on, red) or to tank (off, blue). As the spool rotates, the inlet nozzles, which are stationary on the valve sleeve, transition across the barriers and alternate the flow path between application and tank. The duty ratio, or proportion per PWM cycle that the flow is directed to the application, is controlled by changing the axial position of the spool. By translating the spool upward relative to the inlet, the inlet will remain connected to the tank region for a greater portion per rotation of the spool. This decreases the duty ratio. The opposite effect will occur if the spool is translated downwards relative to the inlet.

The rotary motion of our valve spool is achieved by extracting momentum from the fluid itself as the valve apportions flow to the application and to tank. The sleeve contains an internal pressure rail (see Fig. 4) that feeds tangential inlet nozzles, which create the fluid momentum. As the high speed fluid is transferred from the inlet nozzles to the valve spool, the helical barriers act as turbine blades to capture momentum from the fluid and direct it inward toward the center of the spool. As the fluid is directed inward, the momentum in the fluid is transferred to angular momentum in the spool. Once the fluid is at the center of the spool, it is forced to flow axially through an internal axial passageway that leads to the outlet stage turbine (see Fig. 2). The outlet stage turbine, similar in functionality to a lawn sprinkler, re-accelerates the flow outward and tangential to the spool. The outlet stage reverses the direction of the fluid relative to the inlet stage, which results in a reaction torque on the spool. By utilizing the fluid that must already pass through the valve for actuation, our self-spinning concept does not require an additional power source for operation. The self-spinning design is further enhanced by the 3-way configuration of our valve. The 3-way design continuously feeds fluid through the valve spool regardless of whether the flow is directed to application or tank. This allows the spool to rotate regardless of duty ratio. When combined with a 4-way directional valve, the 3-way functionality of our spool allows the system to operate as both a pump and as a motor.

Our valve is packaged as an integrated pump cover/sleeve that can be bolted directly onto existing fixed displacement pumps. This integrated packaging allows us to minimize the inlet volume between the pump and valve (see Fig. 8), thus reducing energy loss due to fluid compressibility [5]. A diagram of our valve assembly is presented in Figs. 3 and 4. Figure 4 reveals a closer look at the interior geometry of our design as well as illustrates many of the design features.

The remainder of this section includes a description of the spool geometry and design parameters, which is presented in Section 2.1, as well as a discussion of the linear and rotary actuation and sensing, presented in Sections 2.2 and 2.3 respectively.

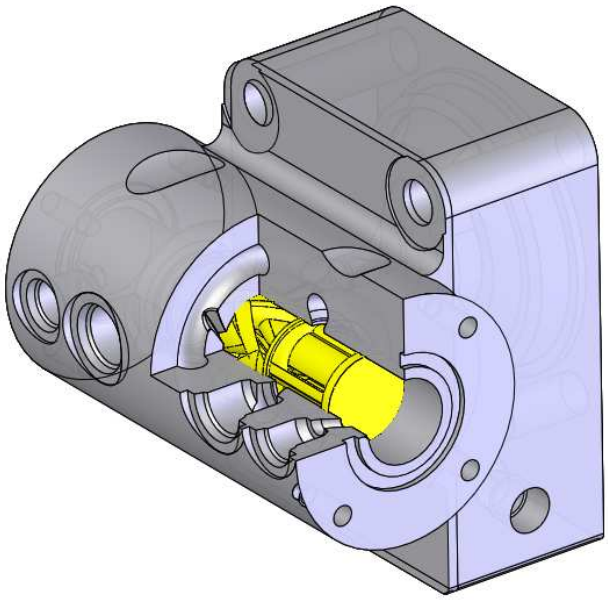

Figure 3. Cutaway rendering of rotary spool/sleeve assembly

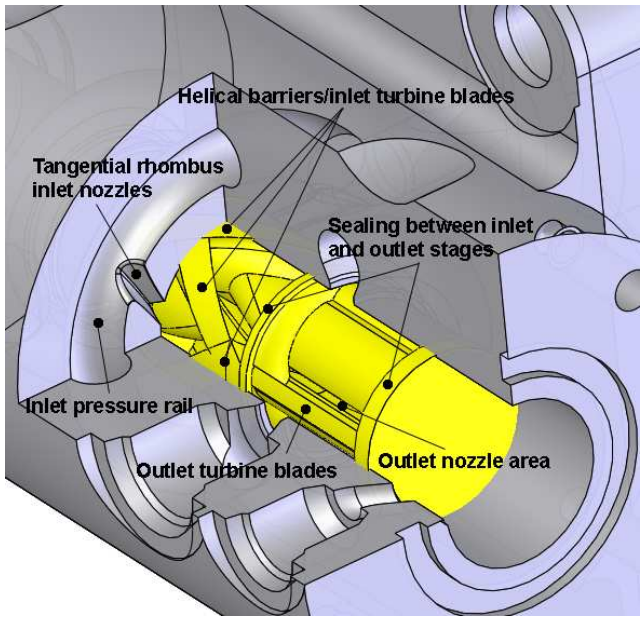

Figure 4. Detailed rendering of rotary spool/sleeve assembly

2.1 Spool Geometry and Design Parameters

The geometry of our spool is presented in Fig. 5, which illustrates the central PWM section of our spool unwrapped from the spool surface. The helical barriers unfold into a triangular sawtooth partition. As the spool rotates, the helical barriers translate across the inlets and fluid is directed from one branch (application or tank) to the other. Note that the central PWM section of

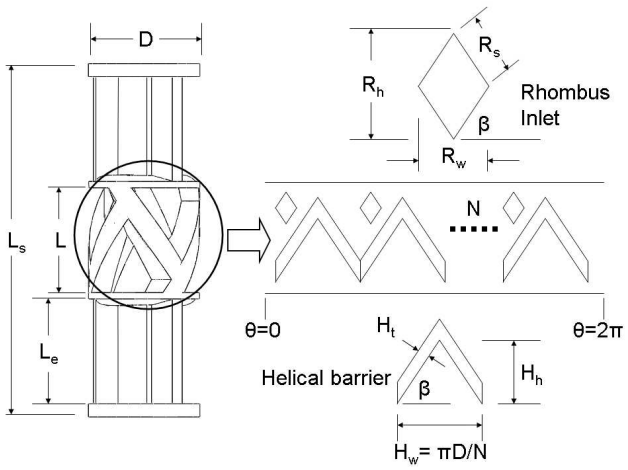

Figure 5. Diagram of unwrapped spool

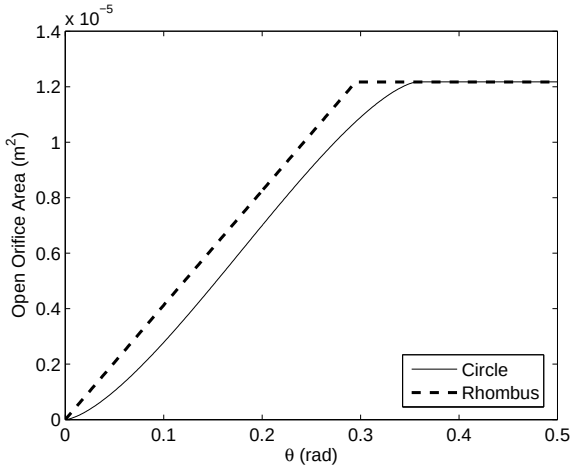

Figure 6. Open orifice area during transition

Parameter	Description
D	Spool diameter
R	Spool radius, $R = \frac{D}{2}$
L_s	Spool length
L	PWM section length
L_e	Exit section length
R_h	Rhombus height
R_w	Rhombus width
R_s	Rhombus side length, $R_s = \frac{1}{2}\sqrt{R_w^2 + R_h^2}$
β	Helix angle
H_h	Helix height
H_w	Helix width
H_t	Helix thickness
N	Number of helices

Table 1. Definition of parameters

the spool is divided into N triangular sections corresponding to N inlets. Each triangular section performs one complete on/off cycle. Therefore, there are N PWM cycles per revolution of the spool and the PWM frequency of the valve is N times the spool frequency. A description of the relevant design parameters for the spool geometry is given in Table 1.

The inlet orifice of our design is shaped as a rhombus with sides of length R_s that are parallel to the helical barriers, as shown in Fig. 5. A rhombus shaped inlet, which has a constant area gradient $\frac{dA}{d\theta}$, provides a faster rate of change in area ($\frac{dA}{d\theta}$) than a circular orifice of equal size during the initial and final stages of transition, which can be seen in Fig. 6. These are the regions where quick transitions are desirable since most throttling losses occur when the inlet orifice is just beginning to open or close.

Four transition events occur every PWM cycle in our 3-way design: opening and closing of the inlet to the load branch, and opening and closing to the tank branch. The proportion of time that the valve is in transition is dependent on the width of the rhombus inlet, R_w, thickness of the helical barriers, H_t, and the number of PWM sections on the spool surface, N. Thus, the proportion of time that the valve is in transition is:

$$\kappa = \frac{2 \cdot N \cdot \left(R_w + \frac{H_t}{\sin(\beta)}\right)}{\pi \cdot D} \tag{1}$$

$0 \leq \kappa \leq 1$. Physically, R_w is constrained such that $0 \leq \kappa \leq 1$ while R_h is constrained by the length of the PWM section of the spool, or $R_h < L$. Ideally, κ must be small to minimize the proportion of each PWM cycle that the valve is in transition. Since our valve is least efficient during transition, decreasing κ will increase the efficiency of our valve. κ can be decreased by setting R_w to be small, or D to be large. Both cases, however, increase the surface area of the spool, which increases viscous friction and decreases the spool velocity.

The sizing of the rhombus shaped inlet orifice area A_{in} and outlet turbine exit area $A_{out} = c_{out} \cdot L_e$ (see Fig. 16) represent a direct trade-off between the spool rotational velocity, valve transition time, and fully-open throttling losses. We define ΔP_{open} to be the pressure drop across the rhombus inlet when it is fully open, and ΔP_{exit} to be the pressure drop across the outlet turbine exit. When ΔP_{open} or ΔP_{exit} is large, more kinetic energy is transferred to the fluid resulting in a higher spool velocity. This speed, however, is attained at the cost of greater throttling

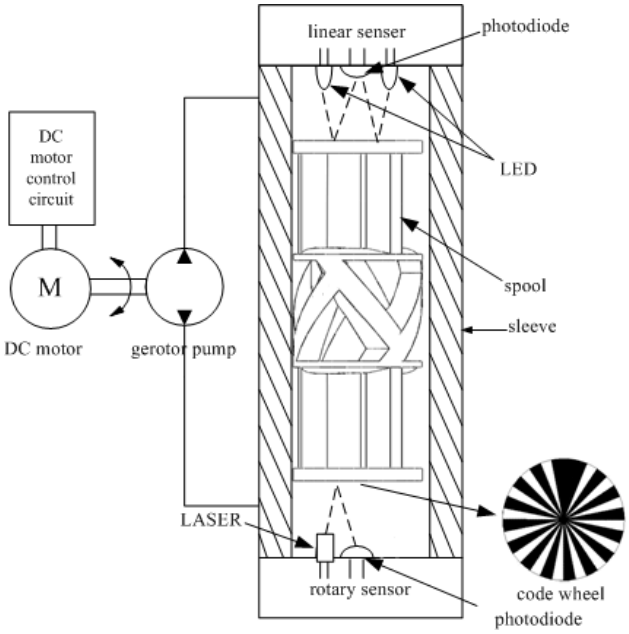

Figure 7. Diagram of linear actuation and rotary sensing system

losses. A_{in} and A_{out} are sized in our current design such that the fully open throttling losses do not exceed some maximum acceptable value. Since the flow rate Q of the system is constant, the maximum throttling loss requirement limits the pressure drop across the inlet and outlet stages, which determines A_{in} and A_{out}. The maximum fully open throttling loss is given by $Power = (\Delta P_{open} + \Delta P_{exit}) \cdot Q$. A_{in} and A_{out} can be calculated using the orifice equation, which is defined as:

$$\Delta P_* = \frac{\rho}{2} \left(\frac{Q}{C_d \cdot A_{total,*}} \right)^2 \tag{2}$$

where * denotes in or out. ρ is the density of hydraulic oil, C_d is the orifice discharge coefficient, and A is the cross-sectional area of the orifice. The height, R_h, and width, R_w, of the rhombus are constrained by the inlet area according to $A_{in} = .5 \cdot R_w \cdot R_h$.

2.2 Linear Actuation and Sensing

The axial position of the spool is actuated hydro-statically using an electro-hydraulic gerotor pump that is hydraulically connected to both ends of the valve sleeve. A schematic of the hydraulic axial position system is presented in Fig. 7. The DC motor is powered by a PWM controlled H-bridge electrical circuit. By pumping fluid from one end of the sleeve to the other, the axial position of the spool can be varied. The gerotor pump flow rate is statically related to the input to the DC motor driving circuit.

The axial position of the spool is measured using a non-contact optical method. A sensor plate with two LEDs and a photodiode is mounted to one end of the valve sleeve. The light emitted from the LEDs is reflected off of the surface of the valve spool and sensed by a photodiode in the sensor plate. The light intensity detected by the photodiode decreases as the distance between the photodiode and spool surface increases. Therefore the position of the spool can be measured from the output voltage of the photodiode.

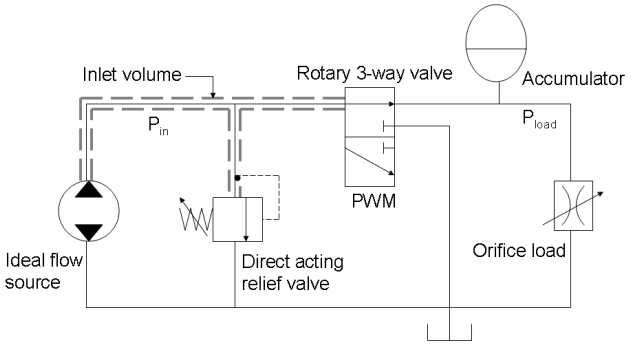

Figure 8. Circuit diagram of PWM variable displacement pump. Load branch includes accumulator and orifice load. Tank branch indicates bypass branch to tank.

2.3 Rotary Sensing

The rotary position and angular velocity of the spool are measured using a similar method to that used for linear sensing. A 30 sector code wheel with an index is attached to one end of the spool. A low-power diode laser module and a photodiode are mounted onto a sensor plate, which is attached to one end of the sleeve. The intensity of the reflected light varies significantly between adjacent sectors. The light intensity detected by the photodiode is transformed into a proportional voltage signal. A counter is used to count the number of changes in voltage amplitude while the index is used to reset the counter. From this information, the position and velocity of the spool can be calculated.

3 Throttling Loss and Flow Analysis

The analysis presented in this section is based upon the system shown in Fig. 8. The system consists of an ideal flow source with flow rate Q, relief valve set at P_{relief}, and a constant application or load pressure of P_{load}. An orifice load is assumed for simplicity in the simulation discussed in Section 4, although other loads can be considered. P_{in} is defined as the pressure in the inlet volume, which is the volume upstream of the valve.

This section is organized as follows: Section 3.1 provides an analysis of the throttling losses experienced by our valve, while Section 3.2 presents the relationship between the spools's axial

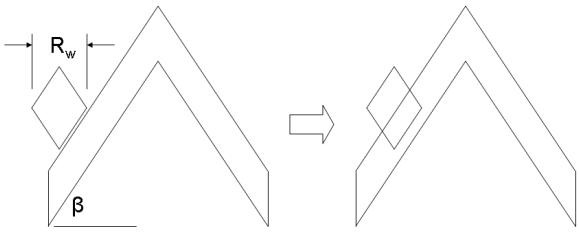

Figure 9. Change in rhombus area during transition

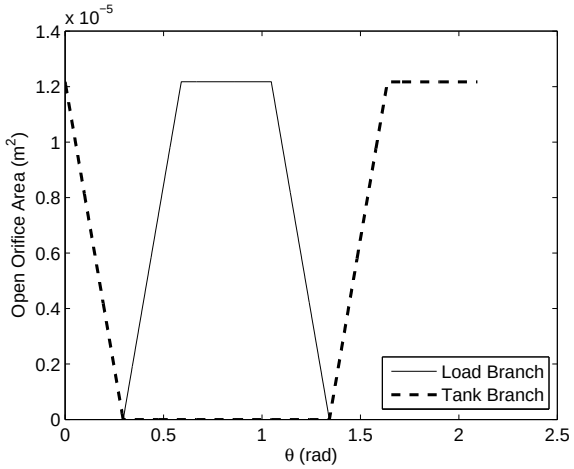

Figure 10. Open orifice area for 1 PWM period

position and flow. Section 3.3 contains a method of estimating the spool velocity and Section 3.4 provides an analysis on the effect of bearing surface area on viscous friction. A preliminary leakage analysis is presented in Section 3.5, and a summary of our design is given in Section 3.6.

3.1 Valve Throttling Losses

Our valve experiences throttling losses that occur across the rhombus inlets and outlet turbine exits when the valve is fully open, as well as increased throttling losses that occur during transitions between application and tank. The inlet pressure profile for one PWM cycle is illustrated in Fig. 11, which corresponds to the area plots shown in Fig. 10. Figures 12 and 13 illustrate the flow profiles and pressure drop across the inlet corresponding to Fig. 10. The total throttling power loss for one PWM cycle can be found by multiplying the curves in Figs. 12 and 13 together. The result is shown in Fig. 14, which reveals that a majority of the energy loss occurs during transition when the relief valve opens and during the two tank transition events.

The fully open loss is determined by the sizing of A_{in} and A_{out} as described in Section 2.1. The fully open loss is estimated by assuming that the full system flow Q enters and exits the valve throughout the entire PWM cycle when the valve is not in tran-

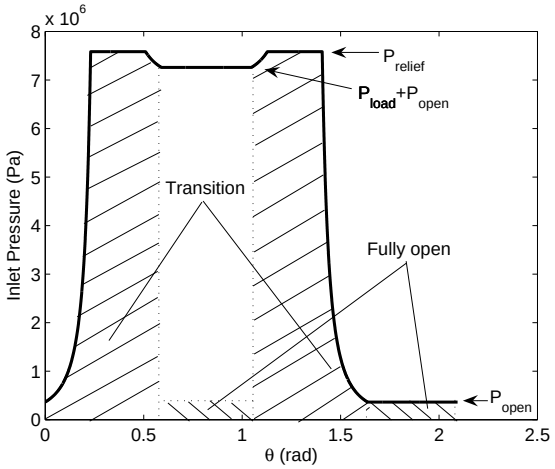

Figure 11. Inlet pressure for 1 PWM period

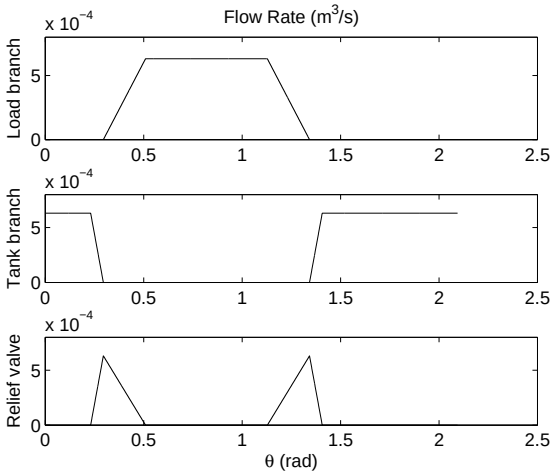

Figure 12. Flow rate through valve for 1 PWM period

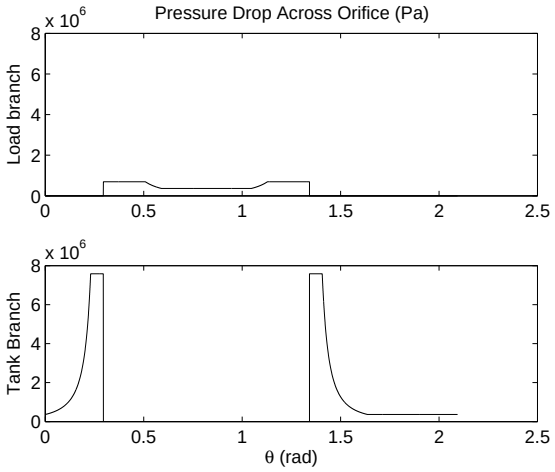

Figure 13. Pressure drop across inlet orifice for 1 PWM period

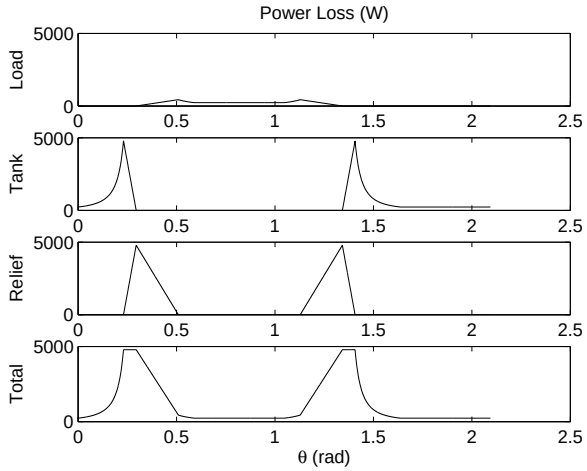

Figure 14. Transition power loss for 1 PWM period

sition. The fully open losses can be estimated by considering ΔP_{open} (pressure drop across the fully open inlet nozzles), ΔP_{exit} (pressure drop across the outlet turbine exits), Q (full system flow), and κ (proportion per rotation the valve is in transition, Eq. (1)):

$$Power_{open} = (1-\kappa)\cdot(\Delta P_{open} + \Delta P_{exit})\cdot Q \tag{3}$$

During transition, throttling losses occur because the valve cannot open and close instantaneously. As a result the inlet orifice is partially open during transition, which induces a large pressure drop across the orifice. Assuming that the spool rotates at a constant angular velocity ω, we expect the transition time for each transition event to be equal and given by:

$$t_{tr} = 2\cdot\left(\frac{R_w + \frac{H_t}{\sin(\beta)}}{D\cdot\omega}\right) \tag{4}$$

To estimate the throttling losses of our valve during transition, we assume that the inlet orifice cannot be simultaneously open to both load and tank, which sets $\frac{H_t}{\sin(\beta)} = R_w$ in Eq. (4). Since t_{tr} is constant, we expect the energy lost during the two transition events involving the load branch (opening and closing) to be equal, and similarly for the two events involving the tank branch. We define ΔP_{on} and Q_{load} to be the pressure drop and flow though the open orifice area A_{open} when the valve is connected to the load branch, and similarly define ΔP_{off} and Q_{tank} for when the valve is connected to tank. A_{open} is a function of the spool's angular position during transition, θ_{tr} (where $d\theta = d\theta_{tr}$), and is determined from geometry to be:

$$A_{open}(\theta_{tr}) = \frac{R_h\cdot D}{4}\cdot\theta_{tr} \tag{5}$$

We let $\theta_{tr} = 0$ to denote the beginning of a transition event, and $\theta_{tr} = \frac{R_w}{R}$ to denote the end of a transition event. We now consider the throttling losses during the two transitions to tank. When the inlet orifice is opening, the initial inlet pressure is high and the relief valve is open. As the open orifice area increases, the pressure begins to decrease until the relief valve closes and the full flow Q is sent through the valve to tank. Initially, when the relief valve is open, the inlet pressure is fixed at P_{relief} and flow is being throttled across both the relief valve and inlet orifice area A_{open}. During this period, flow is throttled across both the relief valve and A_{open} at a pressure drop of P_{relief}. Thus, the energy lost while the relief valve is open is:

$$E_{tr,1} = \int_{t=0}^{t=t_R} Q\cdot P_{relief}\,dt \tag{6}$$

t_R is the time when the pressure at the inlet is equal to P_{relief} and the relief valve is on the verge of closing. We now use the definition of $\omega = \frac{d\theta}{dt}$ to integrate Eq. (6) with respect to θ_{tr}:

$$\begin{aligned} E_{tr,1} &= \frac{1}{\omega}\int_{\theta_{tr}=0}^{\theta_{tr}=\theta_R} Q\cdot P_{relief}\cdot d\theta_{tr} \\ &= \frac{Q\cdot R_w}{\omega\cdot R}\cdot\sqrt{P_{open}\cdot P_{relief}} \end{aligned} \tag{7}$$

θ_R is the angular displacement corresponding to the orifice area that produces P_{relief}. At θ_R, the relief valve closes as the inlet pressure just begins to fall below P_{relief}. θ_R can be calculated using the orifice equation, Eq. (2), and Eq. (5).

Once the inlet pressure drops below P_{relief} and the relief valve closes, the flow through A_{open} is Q and remains constant for the remainder of the transition. ΔP_{off}, the pressure drop across the orifice, is calculated using the orifice equation. The energy loss for the remainder of the transition with the relief valve closed is:

$$\begin{aligned} E_{tr,2} &= \frac{1}{\omega}\int_{\theta_{tr}=\theta_R}^{\theta_{tr}=\frac{R_w}{R}} Q\cdot\Delta P_{off}\cdot d\theta_{tr} \\ &= \frac{Q\cdot R_w}{\omega\cdot R}\cdot\sqrt{P_{open}\cdot(P_{relief}-P_{open})} \end{aligned} \tag{8}$$

The total energy lost during the transition from fully closed to fully open to tank is the sum of Eq. (7) and Eq. (8).

The energy loss during the two transitions involving the load branch are calculated in a similar manner. The main difference is that the inlet pressure is now the pressure drop across the orifice ΔP_{on} plus the load pressure. When the relief valve is open, flow is throttled across P_{relief} through the relief valve, but only across $(P_{relief} - P_{load})$ through A_{open}. We now consider the transition

when the orifice is beginning to open to the load branch. The energy lost during the initial stage of the transition when the relief valve is open is:

$$E_{tr,3} = \frac{1}{\omega}\int_{\theta_{tr}=0}^{\theta_{tr}=\theta_R} (Q - Q_{load}) \cdot P_{relief} \cdot d\theta_{tr} + \frac{1}{\omega}\int_{\theta_{tr}=0}^{\theta_{tr}=\theta_R} Q_{load} \cdot (P_{relief} - P_{load}) \cdot d\theta_{tr} = \frac{Q \cdot R_w}{\omega \cdot R} \cdot \sqrt{\frac{P_{open}}{(P_{relief} - P_{load})}} \cdot \left(P_{relief} - \frac{1}{2}P_{load}\right) \quad (9)$$

Once the relief valve closes, the remaining energy loss during the transition is:

$$E_{tr,4} = \frac{1}{\omega}\int_{\theta_{tr}=\theta_R}^{\theta_{tr}=\frac{R_w}{R}} Q \cdot P_{on} \cdot d\theta_{tr} = \frac{Q \cdot R_w}{\omega \cdot R} \cdot \left(\sqrt{P_{open} \cdot (P_{relief} - P_{load})} - P_{open}\right) \quad (10)$$

The total energy lost during the transition from fully closed to fully open to the load branch is the sum of Eq. (9) and Eq. (10). The total energy lost for all four transition events, or for one complete PWM cycle, is:

$$E_{tr,total} = 2 \cdot (E_{tr,1} + E_{tr,2} + E_{tr,3} + E_{tr,4}) \quad (11)$$

The total power loss due to fully open and transition throttling is:

$$Power_{total} = Power_{open} + E_{tr,total} \cdot \frac{N \cdot \omega}{2 \cdot \pi} \quad (12)$$

3.2 Output Flow vs. Axial Position

The relationship between flow to the load and tank branches with respect to the axial displacement was determined numerically using the Matlab model presented in Section 4. The results are shown in Fig. 15. The central portion of Fig. 15 is linear, which is expected given the linear nature of the helical barrier shown in Fig. 5. Toward the two extremes of the axial travel the flow levels off. This is when the full flow is directed to either load or tank and the inlet does not overlap the barriers at all. In between the linear and level portions of the curve exist nonlinearities, which occur due to the junctions where the barriers intersect. Note that $Q_{load} + Q_{tank} \neq Q$ due to flow through the relief valve during transition. Also note that Q_{load} decreases as P_{load} increases, which is expected since the relief valve opens for a greater proportion of transition for a higher load pressure. This is

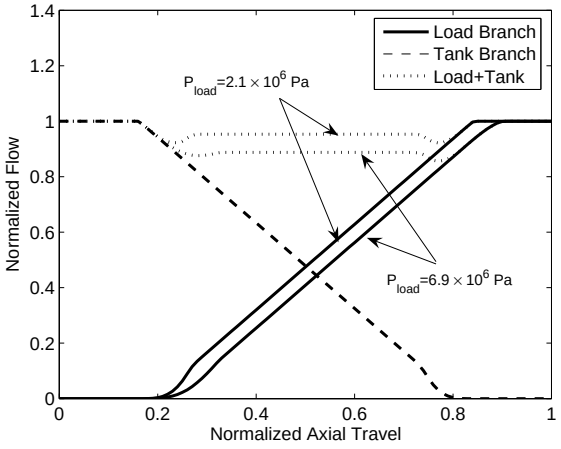

Figure 15. Relationship between flow and axial position

because $P_{in} = \Delta P_{on} + P_{load} \leq P_{relief}$. The total flow, $Q_{load} + Q_{tank}$, in the linear range of the axial travel between $20\% - 80\%$, is especially low (about 90%) due to the relief valve opening during transition, which indicates a significant source of energy loss. Methods to reduce or eliminate the energy lost through the relief valve must be investigated.

3.3 Spool Velocity Analysis

The spool rotational velocity was calculated by considering an angular momentum balance on the spool. The analysis assumes incompressible flow and one-dimensional inlets and outlets. The momentum balance yields:

$$J \cdot \ddot{\theta} = \tau_{in} + \tau_{out} - \tau_f \quad (13)$$

J is the mass moment of inertia of the spool and $\ddot{\theta}$ is the angular acceleration of the spool. τ_{in} is the torque generated by the inlet stage turbine, and τ_{out} by the outlet stage. In the steady state, $\ddot{\theta} = 0$ and the angular momentum generated by the inlet and outlet stages of the spool are balanced by viscous friction.

The resistive torque due to viscous friction was assumed to obey Petroff's Law. Petroff's Law presumes that the torque due to friction is proportional to the bearing surface area, shear stress, and the moment arm where the shear stress acts on the system [2]. Thus, the torque due to friction is given by:

$$\tau_f = A_{eff} \cdot \frac{\mu}{c} \cdot R^2 \cdot \omega \quad (14)$$

R is the spool radius, μ is the dynamic viscosity of hydraulic oil, c is the radial clearance between the spool and sleeve, and A_{eff} is the effective surface area of the spool. The A_{eff} is estimated numerically in Section 3.4 using a simple CFD analysis.

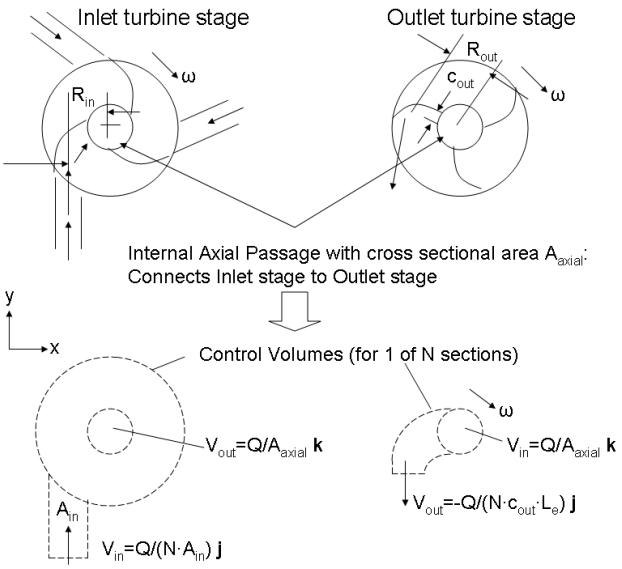

Figure 16. Sketches of the inlet and outlet turbine stages

In our current design, the inlet stage of the valve spool has the functionality of an impulse turbine, and the outlet stage a reaction turbine [3]. A sketch of the inlet and outlet stages of the valve as well as the control volumes that were used is shown in Fig. 16. The inlet stage of the valve consists of N stationary inlet nozzles located on the valve sleeve tangential to the spool. The inlets are offset a distance R_{in} from the center of the spool. In the inlet stage analysis, we consider a stationary control volume that surrounds the spool and inlets. This control volume has N inlets and one outlet, although for simplicity, only one inlet is shown in Fig. 16. At the inlets, angular momentum is generated in the fluid as it enters the control volume tangentially. Since the fluid exits the control volume through an internal axial passage, we assume that the fluid exits with no angular momentum, and that all of the angular momentum generated by the inlets is transferred to the spool. Using this control volume approach, the torque generated by the inlet stage is:

$$\tau_{in} = \sum_{1}^{N} (R_{in} \times v)_{in} \cdot \dot{m}_{in} = \frac{\rho \cdot R_{in}}{A_{in} \cdot N} \cdot Q^2 \tag{15}$$

ρ is the density of hydraulic oil, v is the mean velocity of the fluid as it exits the inlet nozzle, and $\dot{m}$ is the mass flow rate through the nozzle.

By equating $\tau_{in} = \tau_f$, the velocity of the spool generated by the inlet stage alone is:

$$\omega = \frac{\rho \cdot Q^2}{N \cdot R^2 \cdot A_{eff} \cdot \frac{\mu}{c}} \cdot \frac{R_{in}}{A_{in}} \tag{16}$$

The outlet stage of the valve consists of n curved blades that turn the flow as it travels outward. In our current design, $n = N$. In the outlet stage turbine analysis, we neglect the interaction between the spool and sleeve to simplify the analysis, and consider a control volume that rotates with the spool. This control volume consists of one inlet, and N rotating outlets, although only one is shown for simplicity in Fig. 16. Fluid enters the outlet stage axially through the internal axial passage which connects the inlet stage to the outlet stage. Since the fluid enters the stage axially, it is assumed to have no angular momentum as it enters the control volume. As the fluid is directed outward and tangential to the spool surface, a reaction torque is experienced by the spool as it turns the flow. The outlet stage is assumed to be ideal such that the fluid is completely turned by the blades. With this assumption, the outlet stage can be thought of as a rotating tangential outlet nozzle with area $A_{out} = c_{out} \cdot L_e$ offset a distance R_{out} from the center of the spool. The torque generated by the outlet stage is:

$$\tau_{out} = \sum_{1}^{N} (R_{out} \times (v - v_{CV}))_{out} \cdot \dot{m}_{out} = \frac{\rho \cdot R_{out}}{A_{out} \cdot N} \cdot Q^2 - R_{out}^2 \cdot \rho \cdot \omega \cdot Q \tag{17}$$

$v_{CV} = R_{out} \cdot \omega$ is the velocity of the control volume.

Equating the inlet and outlet torque to the friction torque in the steady state produces the equation for ω, the angular velocity of the spool generated by both stages:

$$\omega = \frac{\rho \cdot Q^2}{N \cdot R^2 \cdot (A_{eff} \cdot \frac{\mu}{c} + \frac{R_{out}^2}{R^2} \cdot \rho \cdot Q)} \cdot \frac{R_{in}}{\overline{A}} \tag{18}$$

From Eq. (18), we see that the combined inlet and outlet effects can be normalized such that the system resembles an inlet only configuration. $\overline{A}$ is defined as the equivalent area, and is given by:

$$\frac{1}{\overline{A}} = \frac{1}{A_{in}} + \frac{R_{out}}{R_{in} \cdot A_{out}} \tag{19}$$

Note that setting $R_{out} = 0$ reduces Eq. (18) to the inlet turbine only case.

Eq. (18) illustrates the dual effects of the outlet stage turbine on the spool velocity. $\frac{R_{out}}{R_{in} \cdot A_{out}}$ corresponds to the angular momentum generated by the tangential outlet. Either increasing the moment arm R_{out} or decreasing the outlet nozzle area A_{out} (and thereby imparting more kinetic energy to the fluid at the expense of pressure drop) will increase the spool velocity. The momentum generated by the outlet, however, is counteracted by the additional $\frac{R_{out}^2}{R^2} \cdot \rho \cdot Q$ term, which corresponds to the angular momentum which must be transferred to the fluid as it is forced to

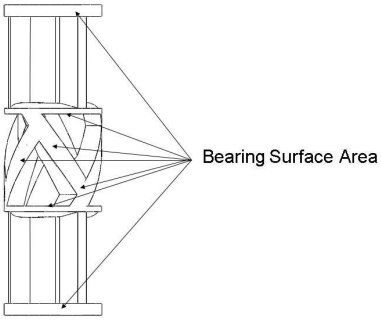

Figure 17. Bearing surface area of valve spool

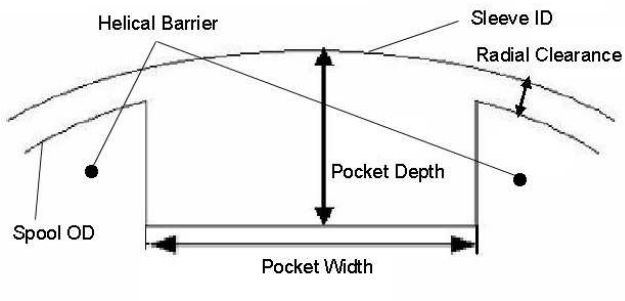

Figure 18. Schematic of pocketed non-bearing surface

rotate with the same circumferential velocity as the outlet blades. As the fluid flows radially outward, more momentum must be transferred to the fluid as the circumferential velocity of the outlet blades increases proportionally with R_{out}. Therefore, increasing the outlet moment arm R_{out} also has the effect of decreasing the spool speed.

The greatest benefit from the addition of the outlet stage turbine is that the effects of the inlet geometry on the PWM functionality of the valve can be decoupled from the spool velocity. By using the outlet stage to provide a majority of the momentum to rotate the spool, the inlet orifice area and thickness of the helical barriers can be optimized for PWM. The only potential issue is whether or not the outlet stage can be designed as effectively as the inlet stage, which resembles the more traditional inflow turbine geometry.

3.4 Effective Bearing Surface Analysis

A simple CFD analysis was performed to calculate the effective bearing surface area of the spool used to calculate the friction torque in Eq. (14). The effective surface area accounts for the contribution of the non-bearing surface area to the friction torque. The non-bearing surface area is defined to be the total surface area $\pi \cdot D \cdot L_s$ minus the bearing surface area, which is shown in Fig. 17. A_{eff} is given by:

$$A_{eff} = A_{bearing} + \alpha \cdot (\pi \cdot D \cdot L_s - A_{bearing}) \qquad (20)$$

α is defined to be the ratio of non-bearing shear stress to bearing surface shear, or $\alpha = \frac{\sigma_{non-bearing}}{\sigma_{bearing}}$. The objective of our CFD analysis is to determine α.

In our current design, the radial clearance c of the spool bearing surface area (as defined in Fig. 17) is $2.54 \times 10^{-5} m$ while the radial clearance for the remaining surface area is $3.175 \times 10^{-3} m$. This is the greatest possible radial clearance (or pocket depth as defined in Fig. 18) while maintaining adequate wall thickness for the internal axial passage between the inlet and outlet turbine stages. Petroff's Law, which assumes a Newtonian fluid where shear stress is inversely proportional to clearance, would predict that the effect of the non-bearing area is negligible. Our previous experiments with a $.0323m$ diameter rotary valve, however, revealed otherwise. This is because the fluid in contact with the non-bearing surface area is trapped in a pocketed area between the helical barriers. The fluid in the pocket will recirculate due to the no-slip conditions at the outer stationary sleeve wall as the spool rotates. These vortices will increase the frictional force in the pocketed area.

In our current design, however, the fluid is not completely trapped between the helical barriers. The inlets between the barriers direct fluid toward the center of the spool. Therefore, we expect less circulation and vorticity in our current design, which should correspond to less friction in the non-bearing surface area. A diagram of a simplified model of the pocketed area is shown in Fig. 18.

Although the actual upper boundary of the domain is curved (sleeve ID) as shown in Fig. 18, we will approximate the upper surface as flat to simplify the analysis. As a further simplification, the system is inverted. Instead of rotating the spool in the simulation, we rotate the sleeve. In the computational domain, this equates to a moving upper boundary. The CFD analysis assumes two-dimensional, steady, incompressible Newtonian flow. The pocket was modeled as a rectangular chamber with a moving upper boundary. The upper boundary was given a velocity that corresponded with our previous valve, a $.0323m$ diameter spool rotating at $27Hz$. Both the depth and width of the pocketed area were explored. A plot of the streamlines generated by the CFD code illustrating the primary vortex of the flow is shown in Fig. 19. The primary vortex accounts for the circulation occurring within the pocket between the helical barriers. The numerical results of the analysis are presented in Figs. 20 and 21. These figures show that the width of the pocket has a negligible effect on the shear stress, while the depth of the pocket is crucial. Therefore, in our current design, we will design the pocket depth, or clearance of the non-bearing area, to be as large as possible while still maintaining adequate wall thickness for the internal axial passage between the inlet and outlet stages. From Fig. 20, for a depth of $3.175 \times 10^{-3} m$, the corresponding

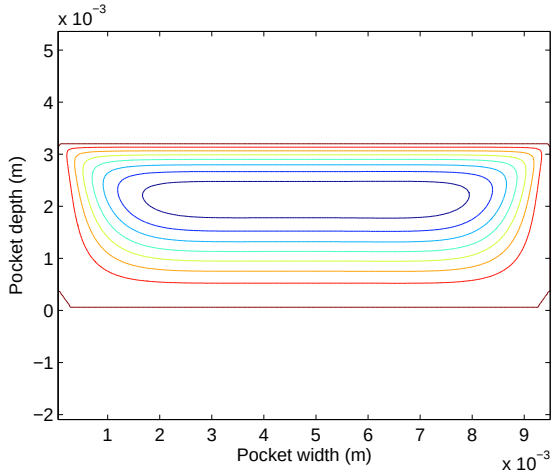

Figure 19. Streamlines within pocket

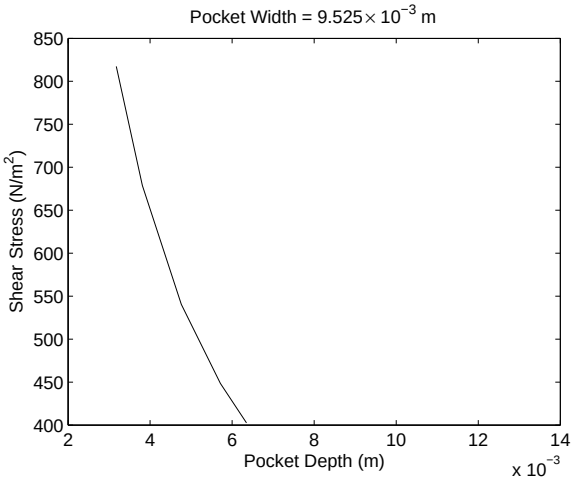

Figure 20. Effect of pocket depth on shear stress

shear stress is predicted to be roughly $820N/m^2 = \sigma_{non-bearing}$. The shear stress for the bearing surface of a $.0323m$ diameter spool rotating at a frequency of $27Hz$ with a radial clearance of $2.54 \times 10^{-5}m$ results in $\sigma_{bearing} = 4169N/m^2$. Therefore, $\alpha = \frac{\sigma_{non-bearing}}{\sigma_{bearing}} = 19.7\%$.

3.5 Leakage Analysis

A preliminary analysis of the internal leakage of the valve was conducted by assuming laminar leakage flow. Since the only feature of the valve that separates high pressure fluid from low pressure fluid is the helical barrier, the valve leakage is assumed to be the flow across this area. The following equation was used

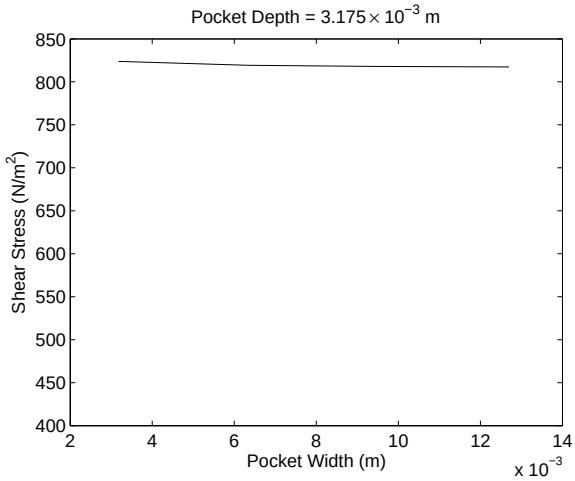

Figure 21. Effect of pocket width on shear stress

to estimate the leakage [4]:

$$Q_{leak} = \frac{Per \cdot c^3 \cdot (P_{load} - P_{open})}{(12 \cdot \mu \cdot H_t)} \tag{21}$$

Per is the perimeter of the leakage surface and c is the radial clearance of the spool as defined previously. This equation indicates a strong relationship between leakage and clearance. A small clearance is desirable to reduce leakage, however a small clearance increases the viscous friction drag on the spool and reduces the spool velocity.

3.6 Design Summary

Several trade offs exist in the design of our self-spinning, 3-way rotary valve concept. Since the rhombus orifice described by Fig. 5 must satisfy:

$$\frac{2 \cdot R_w}{R_h} = \frac{\pi \cdot \frac{D}{N}}{L} \tag{22}$$

and the rhombus area is bound by $A_{in} = \frac{1}{2} \cdot R_w \cdot R_h$, specifying the spool length L and diameter D constrains the rhombus inlet by:

$$\frac{A_{in} \cdot N}{\kappa^2} = \frac{\pi \cdot D \cdot L}{16} \tag{23}$$

Increasing the total inlet area $A_{in} \cdot N$ and decreasing the transition time proportion κ reduce throttling loss. However, Eq. (23) shows that these cannot be done simultaneously without increasing the spool's surface area. In fact, increasing A_{in} at the expense of κ will decrease the total throttling loss. If we wish to decrease

Parameter	SI	English	Description
N	3	–	Number of inlets
D	$.0254m$	$1.0in$	Spool diameter
L	$.0856m$	$3.37in$	Spool length
c	$2.54\times10^{-5}m$	$.001in$	Radial clearance
α	.197	-	Ratio of shear
$A_{bearing}$	$.0015m^2$	$2.39in^2$	Bearing area
A_{in}	$1.22\times10^{-5}m^2$	$.0189in^2$	Inlet rhombus area
A_{out}	$4.68\times10^{-5}m^2$	$.0726in^2$	Turbine exit area
R_h	$.0065m$	$.2558in$	Rhombus height
R_w	$.0037m$	$.1476in$	Rhombus width
β	$1.05rad$	$60deg$	Helix angle
H_t	$.003m$	$.1181in$	Helix thickness
C_d	.6	-	Orifice coefficient
Q	$6.3\times10^{-4}m^3/s$	$10gpm$	Flow rate
P_{load}	6.89×10^6Pa	$1000psi$	Load pressure
P_{relief}	7.58×10^6Pa	$1100psi$	Relief pressure

Table 2. Current system design parameters

the transition losses at the inlet by manipulating A_{in}, ω can be maintained by appropriately specifying A_{out}. Another trade off in our design exists between leakage across the helical barriers and ω. A smaller radial clearance c decreases leakage, but also decreases spool velocity due to increased friction from Eq. (14).

The PWM frequency of our design is proportional to the spool velocity by a factor N. By increasing N, the PWM frequency of our valve can be increased for a given ω. However, N is limited by leakage, as the thickness of the barriers H_t must decrease with N.

Our current prototype is sized for a nominal flow rate of $40l/m$ at a maximum operating pressure of $7Mpa$. Based on the analysis presented in this paper as well as considering manufacturing constraints, the final parameters chosen for our first prototype are summarized in Table 2.

From our current design parameters, we predict that our spool can achieve a rotational velocity of $28Hz$, which corresponds to a PWM frequency of $84Hz$. κ, the proportion of time per revolution that the valve is in transition, is 54.2%. The resisting torque due to viscous friction is estimated to be $0.1116Nm$. From this we estimate that an input power of $19.6W$, which is scavenged from the throttling loss, is needed to overcome viscous friction. The pressure drop across the fully open rhombus inlet and outlet turbine exit are 3.63×10^5Pa and 2.45×10^4Pa respectively. The leakage flow across the helical barriers is $1.26\times10^{-5}m^3/s$ and the total energy lost per PWM cycle due to transition throttling is $13.6J$. Therefore, the total power loss attributed to our valve, which consists of transition and fully open throttling, is $1256W$ which produces a system efficiency of 77.6%.

From the analysis presented in this paper, the majority of power loss is due to throttling during transition. In our 3-way valve configuration, the transition losses are especially high since the number of transition events is doubled in comparison to a 2-way valve. However, the constant flow through the 3-way design is necessary for the self-spinning feature. Improvement in throttling loss can be achieved by increasing the rhombus orifice area through R_h and R_w, and also by increasing the spool dimensions L and D. The PWM frequency can be improved by reducing the effective bearing surface area A_{eff} and by simply increasing N, the number of PWM sections. Additional investigation into the role of the inlet geometry on the transition loss can potentially decrease losses as our current inlet was designed by considering the fully open losses only.

4 Rotary Valve Simulation

A dynamic model of the system shown in Fig. 8 was simulated in Matlab. The system consists of an ideal flow source with a constant flow rate of $6.31\times10^{-4}m^3/s$ and an ideal relief valve set at 7.58×10^6Pa. The accumulator is assumed to be adiabatic with a pre-charge pressure of 6.89×10^5Pa and a pre-charge gas volume of $.16L$. An orifice load described by Eq. (2) with a diameter of $0.0025m$ and discharge coefficient of .7 was used in the model. The current model assumes no fluid compressibility.

The complete system is controlled using a pressure control algorithm proposed by Li et al. [6] of the form:

$$s(t) = K_{ff}\cdot\sqrt{P_{ref}} + K_{fb}\cdot(P_{ref} - P_{out}(t)) \tag{24}$$

$s(t)$ is the desired duty ratio and P_{ref} is the desired reference output pressure. K_{fb}, the feedback gain, was chosen to be .01, which provided a good compromise between responsiveness and overshoot. K_{ff}, the feedforward gain, was calculated to be 2.69×10^{-4} based on an orifice load.

The relationship between duty ratio, $s(t)$, and the axial position of the spool, l, is given in Fig. 15. Inverting the load branch curve in Fig. 15 produces the relationship for calculating the axial position as a function of duty ratio. The axial position of the spool corresponding to the desired duty ratio is regulated by controlling the input to a DC motor PWM driving circuit. The input is given by:

$$\dot{l} = \frac{f(u)}{A_{end}} \tag{25}$$

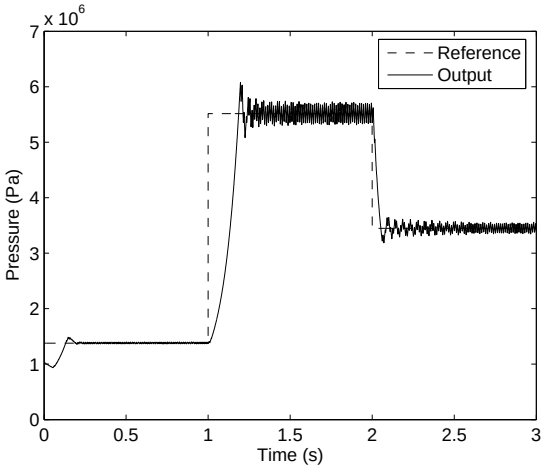

Figure 22. Simulated output pressure

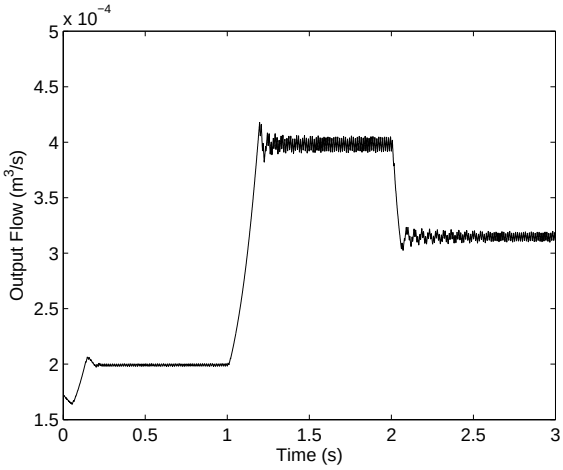

Figure 23. Simulated output flow

u is the input to the DC motor PWM driving circuit, l is the axial position of the spool, and $A_{end} = \frac{\pi}{4} \cdot D^2$ is the area of one end of the spool.

A PI controller with feedforward is used to track l to a reference signal. Both system poles were placed at $-10 rad/s$. Simulations of the axial position controller predict that the controller can reposition the spool from full on to full off in less than $.15s$.

A step reference pressure from $1.38 \times 10^6 Pa$ to $5.52 \times 10^6 Pa$ with a second step to $3.45 \times 10^6 Pa$ was simulated. This input corresponds to a step in flow from $1.99 \times 10^{-4} m^3/s$ to $3.97 \times 10^{-4} m^3/s$ to $3.15 \times 10^{-4} m^3/s$. The system was able to complete the first step in $.19s$ and the second step in $.054s$. The average pressure ripple was 6.67%. The results of the simulation are presented in Figs. 22 and 23, and show that our 3-way rotary valve with hydro-static linear actuation can work effectively to modulate flow.

The response of the simulated system is currently limited by the accumulator. The speed of the system can be increased by either decreasing the pre-charge pressure, or decreasing the precharge volume of the accumulator. Either of these modifications, however, will increase the magnitude of the output pressure ripple. Another alternative is to increase the PWM frequency of the system. This can further improve the response without the penalty in ripple size.

5 Conclusion

A novel 3-way self-spinning rotary on/off valve concept has been presented that is potentially more efficient than a comparable linear valve of equal switching frequency and flow rating. The analysis in this paper predicts that a rotary valve sized for a nominal flow rate of $40 l/m$ can achieve a PWM frequency of $84 Hz$. This frequency is attained by harvesting waste throttling energy from the system flow. No external actuation is needed to rotate the spool in this design.

A complete system model of a PWM variable displacement pump utilizing our 3-way rotary valve has been simulated with promising results. The simulation shows that the hydro-static linear control scheme is effective in controlling the axial position of the spool. The simulation also shows that variable displacement pump functionality utilizing the rotary valve can be achieved by adding closed-loop control to the system.

A number of trade offs between performance and efficiency exist in the design of our rotary on/off valve. The equations presented in this paper provide a means for sizing and optimizing the design based upon physical constraints and efficiency requirements. An analysis of the various modes of power loss in the system reveals that throttling during transition accounts for a majority of the loss in our valve. An opportunity exists to reduce transition losses by optimizing the valve geometry to transition more effectively. κ, the proportion of time that the valve is in transition, needs to be reduced to improve efficiency. This can be achieved by decreasing R_w while keeping the total inlet area A_{in} constant, increasing D, or by having the valve spin selectively faster during transition. Reducing or eliminating the flow throttled across the relief valve during transition will improve efficiency significantly as well. Our design can also be improved by investigating methods of decreasing viscous friction, increasing the number of helical barriers (N), as well as developing a more effective outlet stage turbine.

Acknowledgment

This material is based upon work supported by the National Science Foundation under grant numbers ENG/CMS-0409832 and EEC-0540834.

REFERENCES

[1] F. White, *Fluid Mechanics*. McGraw-Hill, 5th ed., 2003.

[2] A. Cameron, *Basic Lubrication Theory*. John Wiley and Sons, 3rd ed., 1981.

[3] S.L. Dixon, *Fluid Mechanics and Thermodynamics of Turbomachinery*. Elsevier Butterworth-Heinemann, 5th ed., 2005.

[4] J. Cundiff, *Fluid Power Circuits and Controls*. CRC Press, 2002.

[5] M. Rannow, H. Tu, P. Li and T. Chase, "Software Enabled Variable Displacement Pumps - Experimental Studies" *Proceedings of the 2006 ASME-IMECE*, no. IMECE2006-14973, 2006.

[6] P. Li, C. Li and T. Chase, "Software Enabled Variable Displacement Pumps" *Proceedings of the 2005 ASME-IMECE*, no. IMECE2005-81376, 2005.

[7] S. Yokota and K. Akutu, "A Fast-Acting Electro-Hydraulic Digital Transducer (A Poppet-Type On-Off Valve using a Multilayered Piezoelectric Device)," *JSME International Journal, Series 2: Fluids Engineering, Heat Transfer, Power, Combustion, Thermophysical Properties*, vol 34, no. 4, pp. 489–495, 1991.

[8] T. Kajima, S. Satoh and R. Sagawa, "Development of a high speed solenoid valve," *Transactions of the Japan Society of Mechanical Engineering: Part C*, vol. 60, no. 576, pp. 2744–2751, 1994.

[9] H. Lu, C. Zhu, S. Zeng, Y. Huang, M. Zhou and Y. He, "Study on the new kind of electro-hydraulic high speed on-off valve driven by PZT components and its powerful and speedy technique," *Chinese Journal of Mechanical Engineering*, vol. 38, no. 8, pp. 118–121, 2002.

[10] Y. Shi, Y. Zhang, and C. Liu, "Study and design of a high-speed on-off valve taken rare earth alloy matherial as actuator," *Journal of Nanjing University of Science and Technology*, vol. 28, no. 4, pp. 385–384, 2004.

[11] Y. Shi, C. Liu, and Y. Zhang, "Design and study of a new kind of larger flow rate high-speed on-off valve," *Chinese Journal of Mechanical Engineering*, vol. 40, no. 4, pp. 195–198, 2004.

[12] I. Cyphelly and J. Langen, "Ein neues energiesparendes Konzept der Volumenstromdosierung mit Konstantpumpen" *Aachener Fluidtechnisches Kolloquium*, 1980.

[13] T. Royston and R. Singh, "Development of a Pulse-Width Modulated Pneumatic Rotary Valve for Actuator Position Control" *Journal of Dynamic Systems, Measurement, and Control-Transactions of the ASME*, vol. 115, pp. 495–505, 1993.

[14] P. Cui, R. Burton and P. Ukrainetz, "Development of a High Speed On/Off valve," *SAE Technical Paper Series*, pp. 21–25, 1991.